NASA
Technical Memorandum 82964

AVRADCOM
Technical Report 81-C-27

Effect of Steady-State Pressure Distortion on Inlet Flow to a High-Bypass-Ratio Turbofan Engine

Ronald H. Soeder
Lewis Research Center
Cleveland, Ohio

and

George A. Bobula
Propulsion Laboratory
AVRADCOM Research and Technology Laboratories
Lewis Research Center
Cleveland, Ohio

October 1982

DISCLAIMER NOTICE

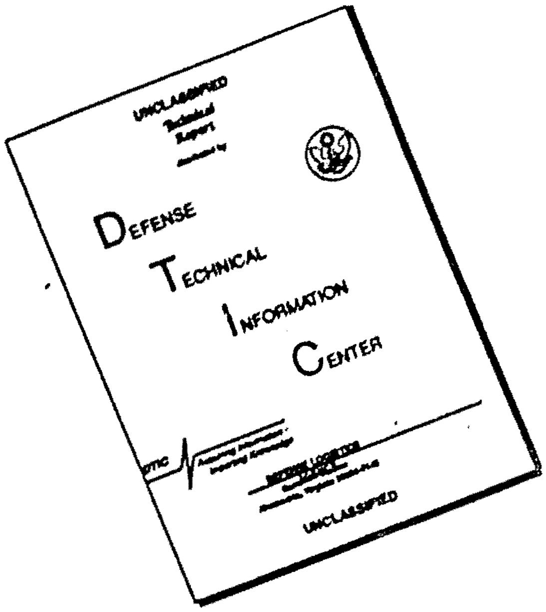

THIS DOCUMENT IS BEST QUALITY AVAILABLE. THE COPY FURNISHED TO DTIC CONTAINED A SIGNIFICANT NUMBER OF PAGES WHICH DO NOT REPRODUCE LEGIBLY.

EFFECT OF STEADY-STATE PRESSURE DISTORTION ON INLET FLOW TO A HIGH-BYPASS-RATIO TURBOFAN ENGINE

Ronald H. Soeder
National Aeronautics and Space Administration
Lewis Research Center
Cleveland, Ohio 44135

and

George A. Bobula
Propulsion Laboratory
AVRADCOM Research and Technology Laboratories
Lewis Research Center
Cleveland, Ohio 44135

E-1383

SUMMARY

Experiments were conducted to determine the effects of steady-state circumferential-pressure distortion on inlet flow and internal engine performance of a high-bypass-ratio turbofan engine. To measure these effects, flow-angle, static-pressure, and total-pressure instrumentation was placed between the rotatable distortion-generator assembly and the engine inlet. In addition, both static-pressure and total-pressure were recorded at the fan exit and compressor inlet and exit. Three circumferential screens were separately mounted on the rotatable assembly. For all configurations data were recorded at each of twelve 30° increments of assembly rotation. Experiments were conducted with fan speeds (corrected to station 2 temperature) of 80 or 90 percent of rated condition (7005 rpm) and Reynolds number indices of 0.2 or 0.5.

Yaw angle increased between the distortion-generating assembly and the engine inlet. A change in Reynolds number index (RNI) had only a slight effect and a change in speed had no effect on yaw angle distribution. The flow angle was largest in the hub region of the engine inlet.

Along the inlet-duct wall, static-pressure distortion generated by the screen assembly increased exponentially as flow approached the engine inlet. Total-pressure distribution displayed no axial variation between the distortion-generating assembly and engine inlet for any of the screens tested. Both total-pressure and static-pressure distortion were attenuated between engine inlet and compressor exit.

INTRODUCTION

A series of investigations was undertaken at the Lewis Research Center to obtain an experimental data base for use in determining the effects of inlet-pressure distortion on engine performance (refs. 1 to 3). In order to reduce the amount of expensive test time for new engine development, a proposal was made to develop analytical compressor models using existing experimental data. The function of these models was to predict the effects of inlet distortion on the operating characteristics of turbofan engines. To date, an operational model exists for a low-bypass-ratio turbofan engine (refs. 4 to 6).

This investigation was conducted to further evaluate inlet flow characteristics caused by pressure distortions of different extents and intensities and to provide initial data for a high-bypass-ratio compressor model which is in the developmental stage. In order to properly evaluate this series of inlet-distortion experiments, surveys of total pressure, static pressure, and total temperature were made on a YTF34 turbofan engine at the inlet, the fan exit, and the compressor inlet and exit. Free-stream yaw flow angles were measured using flow-angle rakes at two axial stations between the distortion device and the fan inlet. Static pressures were also installed along the inlet-duct wall at two circumferential positions. Static-pressure variation upstream of an engine inlet is discussed in reference 7.

Data are presented for two engine fan speeds of 80 and 90 percent of rated condition (7005 rpm). Both fan-speed conditions were corrected to station 2 temperature levels. The Reynolds number indices (RNI) were 0.2 and 0.5 (based on the undistorted sectors at the engine inlet). The distortion extents were 90° and 180°, and the screens utilized in the experiments produced total-pressure distortions from 7.1 to 9.8 percent.

SYMBOLS

e	natural logarithm base
M	Mach number
NFR2	fan speed corrected to station 2 test conditions, $NF/\sqrt{\theta_2}$, rpm
P	pressure, Pa
PNFR2	fan speed corrected to station 2 test conditions as a percent of 7005 rpm
RNI	Reynolds number index, $\delta/(\mu/\mu_{sls})\cdot\sqrt{\theta}$
r_m	mean radius of inlet duct, 0.56 m
T	temperature, K
U	tangential velocity, m/sec
V	axial velocity, m/sec
x	axial length, m
β	yaw angle, deg
γ	ratio of specific heats
Δ	maximum-minimum value
δ	ratio of total pressure to standard sea level static pressure
μ	absolute viscosity, kg/(m-sec)

Subscripts

s	static condition
sls	standard sea level static condition
T	total condition

Stations

1	airflow metering station, located 126.64 cm upstream of the engine inlet
1B	yaw measurement station behind the distortion screen, located 57.62 cm upstream of the engine inlet
1C	end of static pressure taps along the inlet-duct wall, located 56.49 cm upstream of the engine inlet
2	engine inlet-pressure, temperature, and flow-angle measurement, located 14.96 cm upstream of the engine inlet
2A	start of static pressure taps along the inlet-duct wall, located

	3.81 cm upstream of the engine inlet
2C	compressor inlet; outer wall of the passage located 57.91 cm downstream of the engine inlet, inner wall of the passage located 55.93 cm downstream of the engine inlet
2.4	fan exit located 30.80 cm downstream of the engine inlet
2.5	inlet to gooseneck passage; outer wall of the passage located 40.30 cm downstream of the engine inlet, inner wall of the passage located 37.25 cm downstream of the engine inlet
2.6	gooseneck passage; outer wall of the passage located 46.88 cm downstream of the engine inlet, inner wall of the passage located 43.42 cm downstream of the engine inlet
2.7	gooseneck passage; outer wall of the passage located 52.53 cm downstream of the engine inlet, inner wall of the passage located 49.72 cm downstream of the engine inlet
3	compressor exit located 121.23 cm downstream of the engine inlet

APPARATUS

Engine

The engine used for this investigation was a YTF34 turbofan, which is a high-bypass-ratio (6.23 to 1) front-fan engine. A single-stage fan, with a pressure ratio of 1.51 to 1, was driven by a four-stage low-pressure turbine. The 14 stage axial flow compressor had a nominal compression ratio of 14.5 to 1 and was driven by a two-stage air-cooled, high-pressure turbine. The engine was installed in an altitude chamber by a direct-connect type of installation (fig. 1). Engine schematic and instrumentation-station diagrams for the region upstream of the fan inlet and at the inlet and exit of the compressor are presented in figure 2.

Distortion Device

Inlet pressure distortion was generated using one of three screen configurations with extents of 90° or 180°. A given screen was mounted on a motor-driven rotatable screen assembly (fig. 3) located 0.692 m (27.24 in) upstream of the engine inlet. Distortion screen descriptions are given in table I.

Instrumentation

The instrumentation used to acquire the data is outlined in figures 2, 4, and 5. Total and static pressures were recorded by means of scanivalves calibrated for a range 0 to 103 kPa (15 psia). These measurements included pressure from just behind the distortion screen to the compressor inlet. In addition, one scanivalve was calibrated for the range 103 to 1276 kPa (15 to 185 psia) to measure pressures at the compressor exit.

Figure 5 shows the details associated with the yaw flow-angle pressure-measurement rake located at station 2. Yaw angle is positive when the tangential flow component is in the direction of fan rotation, as noted on figure 5. A flow-angle measurement rake was also located immediately behind the screen assembly. Flow-angle probes were calibrated for a range of ±30° at the same free-stream Mach numbers encountered during engine experiments. The estimated systematic error is ±2/3° and the random error is ±1/2°. A more detailed description of flow-angle probes is found in reference 8.

Procedure

A motor-driven rotatable screen assembly containing a circumferential distortion screen was rotated a full revolution in twelve 30° increments. After each increment and upon achieving steady-state engine operation, a data point was recorded. Beginning at 0, the first data point was plotted at its angular rake (or tap) position. The second data point was then plotted at an incremental step of 30°, but in a direction opposite to screen-assembly rotation. This procedure is similar to holding the screen assembly in a fixed position and rotating the instrumentation rakes. All pressure data were normalized to upstream plenum pressure to compensate for minor run-to-run variations. This pressure adjustment included pressure measurements made upstream of the engine inlet, the fan exit, and the compressor inlet and exit stations.

The inlet flow angle described in this investigation includes only yaw angle. Pitch-angle measurements were not recorded since the low-bypass-ratio turbofan experiments discussed in reference 9 showed that yaw-angle variations were much larger than pitch-angle variations for a given screen configuration.

For each static tap at two circumferential locations along the inlet-duct wall (see fig. 4), a maximum and minimum static pressure was identified for each test series of 12 data points. The difference between this maximum and minimum was normalized with a similar difference at the static taps nearest the engine inlet (station 2A-fig. 4) and presented as a relative static-pressure distortion level.

The RNI for each test run was held constant (at 0.2 or 0.5) upstream of the distortion-generating device by maintaining approximately a 289 K (520°R) inlet total temperature and adjusting inlet total pressure.

RESULTS

The effects on inlet flow of 90° and 180° steady-state pressure distortion screens at total-pressure distortion levels of 7.1 to 9.8 percent were investigated. The engine inlet RNI was 0.2 or 0.5, and the corrected fan speed was 80 or 90 percent of 7005 rpm (the rated condition). The influences of distortion level and extent, RNI, and fan speed on inlet flow angle, inlet-total and static-pressure distortion, and internal compressor performance are presented in this section.

Flow Angle

Clean inlet. - The undistorted streamline yaw flow angles at the entrance to the engine inlet as functions of corrected fan speed are shown in figure 6. The yaw angle at station 2 varied from 0° at the hub to -2.2° at the tip. Flow angle is independent of speed at any radial location.

180° distortion. - Flow-angle data obtained when the corrected fan speed was 80 or 90 percent of rated condition are presented in figures 7 to 12. The distortion screens used in the experiments had blockages of 40.2 to 49.4 percent (total-pressure distortion from 7.1 to 9.8 percent). Total-pressure distortion at station 2 is defined as

$$(P_{T,max} - P_{T,min})/P_{T,av} \tag{1}$$

The maximum- and minimum-pressure values in the equation refer to a rake average value. The average-pressure term refers to a face average value. The total-pressure distortion values for all screens tested are found in table II.

The yaw-angle tip and midspan profiles behind the screen, located 57.62 cm (22.69 in.) upstream of the engine inlet, were nearly constant with relative circumferential position and were equal to a mean value of -1.2°, as seen in figure 7. Both tip and midspan profiles have been adjusted for clean inlet conditions by subtracting the clean inlet values (fig. 6) from the experimental yaw-angle data. Little difference occurred between tip and midspan profiles (fig. 7); these flat profiles resulted from an absence of engine-pumping effects at station 1B (located immediately behind the screen). As flow approached the engine inlet, the yaw flow angle had a much larger magnitude (fig. 8), and significant variation occurred from tip to hub. (All profiles in figs. 8 to 12 have been adjusted for clean inlet conditions.)

At station 2, 14.96 cm (5.89 in.) upstream of the engine inlet, the largest variation in the hub region occurred with a flow angle range from $+24.3^\circ$ to -22°. The tip and midspan flow angles had nearly identical profiles, with a flow-angle band of $+12.5^\circ$ to -9.5°. The station 2 hub-yaw-angle profile exhibited a larger flow-angle variation than the tip and midspan yaw angles; this resulted from greater engine-pumping effects and larger flow-angle redistributions in the hub region of the engine inlet. Regions of decreasing flow angle at station 2 are indicated in figures 8 to 12 by data plotted within the circumferential region occupied by the distortion screen.

Speed and Reynolds number index effects. - The effect of decreasing fan speed (airflow) from 90 to 80 percent on station 2 yaw angle using a 49.4 percent blockage screen (9.8 percent total-pressure distortion) is presented in figure 9. A decrease in percent-corrected fan speed had essentially no effect on yaw angle between the tip and hub regions at station 2. The hub region at station 2 (see fig. 9(c)) provided the largest variation in flow-angle profile (fig. 8).

The RNI effects on inlet-flow yaw angle at station 2 are presented in figure 10. Pressure distortion was produced by the same 180° screen at 80 percent of rated fan speed. Yaw-angle variation as the RNI was decreased from 0.5 to 0.2 was slightly influenced. Here, as in figure 8, the yaw-angle variation in the hub region was twice the variation of the tip and midspan regions at station 2.

Distortion magnitude and extent effects. - An increase in screen blockage (total-pressure distortion) resulted in increased yaw-angle variation at station 2, as shown in figure 11. The hub region (see fig. 11(c)) showed the largest yaw-angle change. The large hub-region variation was discussed in conjunction with figure 8. The tip and midspan yaw-angle variations were nearly equal. Observe that flow-angle variation increased as the screen blockage (total-pressure distortion) increased. The streamlines of air underwent flow redistribution from the undistorted free-stream sector of the inlet duct to the region of low pressure behind the screen.

The effect of screen extent on yaw angle is shown in figure 12. The largest yaw-angle variation occurred in the hub region (see discussion on fig. 8) An examination of the yaw angle profiles at the tip, midspan, and hub regions shows that the 90° screen produced a larger gradient over the first 90° circumferential sector due to flow redistribution effects.

STATIC-PRESSURE DISTORTION

Static-pressure distortion change along the inlet-duct wall from behind the distortion device to the engine inlet (see fig. 4) is presented in figures 13 to 16. The variables included percent change in corrected fan speed, RNI, screen blockage, and screen extent. The static-pressure distortion change developed in reference 7 and presented in references 5 and 9 for a low-bypass-ratio turbofan engine was found to hold for the high-bypass-ratio turbofan engine used in this investigation. The distortion change is defined as $(P_{s,max} - P_{s,min})$ at station 2A or $(\Delta P_s)/(\Delta P_s)2A$.

The figures noted above show that the relative static-pressure distortion did follow an exponential curve, as discussed in reference 7. The term (x/r_m) is a normalized distance parameter equal to the axial distance along the inlet duct divided by the mean radius of the inlet duct. In figures 13 to 16 the data diverged from the exponential curve at (x/r_m) values of 0.26 and 1.03. These locations represent the axial location for station 2 rakes and the station 1B flow-angle rake which produced disruptive effects on air flow due to rake blockage of the inlet duct.

Examination of the data presented in figures 13 to 16 shows that fan speed, RNI, screen blockage, and screen extent all had minor influence on static-pressure distortion. All data presented are for the case of the first harmonic. The theoretical curve shown in figures 13 to 16 can be mathematically expressed as

$$\frac{\Delta P_s}{(\Delta P_s)_{2A}} = e^{-[n(x-x_{2A})]/r_m} \tag{2}$$

The first harmonic occurs when n in the above expression is equal to one. Other harmonics are discussed in references 7 and 9. The data presented in the figures were obtained from the static taps located at 55°. Data from the taps located at 235° show similar results.

Pressure Profiles at Inlet

The axial variation in free-stream-rake average total pressure between station 1B (behind the screen) and station 2 (engine inlet) and the axial variation of static pressure along the inlet-duct wall from station 1C (56.49 cm upstream of the engine inlet; see fig. 4) to station 2, is presented in figure 17.

The total-pressure remained at a constant level with axial distance (fig. 17(a)). The static-pressure profile had a sinusoidal configuration which increased in amplitude from station 1C (behind the screen) to station 2A (3.81 cm upstream of the engine inlet) (fig. 17(b)). The increase in static-pressure amplitude with axial distance was supported by the discussion in the Static-Pressure Distortion section.

Percent of corrected fan speed, RNI, and screen blockage had a minor effect on total-pressure and static-pressure amplitude along the inlet duct between the distortion screen and engine inlet (figs. 18 to 20).

Compression System Pressure and Temperature Profiles

The variation in total and static pressure and total temperature with relative circumferential position at stations 2.4 (fan exit), 2C (compressor inlet), and 3 (compressor exit) is presented in figures 21 to 23. Examination of the total-pressure profiles in figures 18 to 23 shows that the amplitude of the normalized profiles increased between stations 2 and 2C (compressor inlet); the profiles then attenuated across the compressor. The flat total-pressure profile at station 3 indicated a very small level of total-pressure distortion.

Similarly, a comparison of normalized static-pressure profiles (figs. 18 to 23) shows that the profiles were attenuated across the fan as streamlines of air were introduced into a large, unrestricted volume at the fan exit. The increased area reduced the average static-pressure value (engine core plus fan duct) at a given circumferential position. The normalized static-pressure profile at the compressor exit was relatively flat, which indicates that the level of static-pressure distortion at station 3 was minimal.

The normalized total-temperature profiles at stations 2.4 and 2C were nearly identical. The increase in temperature profile amplitude at station 2.4 with respect to the flat profile at station 2 (not shown) resulted from the greater pressure ratio in the distorted, that is, the lower total-pressure sector of the fan. The temperature profile at station 3 was sinusoidal with increased amplitude compared with stations 2.4 and 2C, again the result of the increased pressure rise in the distorted sector.

The statement regarding the shape of the total- and static-pressure and total-temperature profiles is also valid for changes in fan speed, RNI, and different screen blockages. The data presented in figure 22 showing the RNI effect on pressure and temperature profiles at stations 2, 2.4, 2C, and 3 were obtained with a corrected fan speed of 80 percent of rated condition. An attempt to test the engine at a fan speed of 90 percent of rated condition with RNI at station 2 equal to 0.2 would have resulted in the violation of an interstage-turbine temperature limit.

Normalized static-pressure profiles at stations 2.5, 2.6, and 2.7 (the gooseneck region between the fan exit and the compressor inlet) are shown in figures 24 to 26. Percent of corrected fan speed, RNI, and screen blockage had only minor effects on the profiles. Between stations 2.4 (see figs. 21 to 23) and 2.5, the amplitude of the sinusoidal profiles increased. This increase resulted from the reduction in area from the fan exit to the gooseneck region (upstream of the compressor inlet). The static-pressure profiles remained nearly constant along the gooseneck region.

Variations in Compression-System Distortion

The amplification or attenuation of total-pressure and static-pressure distortions is shown in figures 27 to 29. These profiles were generated using maximum and minimum total-pressure rake averages or static-pressure tap values along with face-average conditions at each instrumented engine station. The data in all three figures show that the total-pressure distortion increased between the engine inlet and the compressor inlet. Total-pressure distortion at station 2.4 for core-pressure variation and at station 2.C was approximately 9 and 9.8 percent, respectively. The total-pressure distortion was nearly attenuated at the compressor exit. The near-zero level of distortion at station 3 is noted by the flat total-pressure profiles in figures 21 to 24.

Static-pressure distortion decreased between the engine inlet and fan exit when static-pressure measurements in the engine core at station 2.4 were used in the distortion computation. The core area was smaller than the core-plus-fan-duct area at the fan exit; therefore, the static-pressure variation in the core was not large. The static-pressure distortion in the core region of the fan exit was approximately 1.5 percent. The level of static-pressure distortion along the gooseneck region of the engine continued to increase with respect to the distortion level at the fan-core exit. The static-pressure distortion at station 2C (compressor inlet) was approximately 8.5 percent and was attenuated at the compressor exit to almost zero.

Total-temperature distortion profiles were not presented in figures 27 to 29 due to the small amplitudes. The temperature distortion level at station 2 was zero and the percent distortion at stations 2.4, 2C, and 3 was in the range of 1.5 to 2 percent.

The data presented in all three figures were recorded with the distortion screen in the 0 to 180° position (clockwise) as viewed in the upstream direction from the engine exhaust. Distortion results with the screen positioned from 90° to 270°, 180° to 360°, or 270° to 90° were essentially the same as the data presented in figures 27 to 29 and therefore are not shown.

SUMMARY OF RESULTS

A TF34 high-bypass-ratio turbofan engine was tested with inlet circumferential-pressure distortion. The results of the experiments are as follows:

1. Yaw angle variation increased as air flow approached the engine inlet.
2. Yaw angle variation was largest in the hub region of the engine inlet for all the screen configurations tested.
3. Variations in corrected fan speed and RNI had a minor effect on yaw angle.
4. For the screens tested, yaw angle increased with increases in screen blockage and screen extent.
5. Screen-induced static-pressure distortion increased exponentially between the distortion-generating assembly and the engine inlet. Variations due to changes in fan speed, RNI, screen blockage, and screen extent had a minor influence on the shape of the curves.
6. Inlet static-pressure distortion amplitudes predicted for a low-bypass-ratio turbofan engine were also applicable for a high-bypass-ratio turbofan engine.
7. Screen-induced total-pressure circumferential profiles remained constant along the inlet duct between the distortion device and the engine inlet. Fan speed, RNI, and screen blockage did not produce variations in the profiles.
8. Normalized total-pressure circumferential profiles varied from a square wave at the engine inlet to a nearly flat profile at the compressor exit.
9. Normalized static-pressure circumferential profiles varied from sinusoidal wave at the engine inlet to a flat profile at the compressor exit.
10. The amplitude of normalized total-temperature circumferential profiles increased from the fan exit to the compressor exit.

11. Total-pressure distortion increased between the engine inlet and the compressor inlet. The distortion level was nearly zero at the compressor exit.

12. Static-pressure distortion decreased between engine inlet and fan core exit. The distortion increased from the fan-core exit to the compressor inlet and was nearly zero at the compressor exit.

REFERENCES

1. Evans, D.G.; et al.: Some Comparisons of the Flow Characteristics of a Turbofan Compressor System with and without Inlet Pressure Distortion. NASA TM X-71574, 1974.
2. de Bogdan, C.E.,; et al.: Effect of a 180° Extent Inlet Pressure Distortion on the Internal Flow Conditions of a TF30-P-3 Engine. NASA TM X-3267, 1975.
3. de Bodgan, C.E.; Moss, J.E., Jr.; and Braithwaite, W.M.: Internal Flow Characteristics of a Multistage Compressor with Inlet Pressure Distortion. NASA TM X-3446, 1977.
4. Mazzawy, R.S.: Multiple Segment Parallel Compressor Model for Circumferential Flow Distortion. J. Eng. Power, vol. 99, no. 2, Apr. 1977, pp. 288-296.
5. Mazzawy, R.S.; and Banks, G.A.: Modeling and Analysis of the TF30-P-3 Compressor System with Inlet Pressure Distortion. (PWA-5302, Pratt & Whitney Aircraft; NASA Contract NAS3-18535). NASA CR-134996, 1976.
6. Mazzawy, R.S.; and Banks, G.A.: Circumferential Distortion Modeling of the TF30-P-3 Compression System. (PWA-5448, Pratt & Whitney Aircraft; NASA Contract NAS3-18535). NASA CR-135124, 1977.
7. Plourde, G.A.: and Stenning, A.H.: Attenuation of Circumferential Inlet Distortion in Multistage Axial Compressors. J. Aircraft, vol. 5, no. 3, May-June 1968, pp. 236-242.
8. Dudzinski, T.J.; and Krause, L.N.: Flow-Direction Measurement with Fixed-Position Probes. NASA TM X-1904, 1969.
9. Soeder, R.H.: and Bobula, G.A.: Effect of Steady-State Pressure Distortion on Flow Characteristics Entering a Turbofan Engine. NASA TM-79134, 1979.
10. Braithwaite, W.M.; and Soeder, R.H.: Combined Pressure and Temperature Distortion Effects on Internal Flow of a Turbofan Engine. NASA TM-79136, 1979.

TABLE I. - SCREEN DESCRIPTION

Screen	Wire diameter, cm	Wire diameter, in.	Width of opening, cm	Width of opening, in.	Blockage, percent	Extent deg
1	0.081	0.032	0.201	0.079	49.4	180
2	.081	.032	.236	.093	44.6	180
3	.089	.035	.302	.119	40[illegible]	180
4	.081	.032	.201	.079	4[illegible]	90

TABLE II. - SCREEN TOTAL-PRESSURE DI[illegible]ON

Screen	Corrected fan speed, PNFR2, percent	Reynolds number index RNI_1	$\frac{P_{T,max} - P_{T,min}}{P_{T,av}}$, percent (a)
1	80	0.2	7.9
		.5	7.7
	90	.5	9.8
2		.5	8.8
3		.5	7.1
4		.5	7.8

(a) $P_{T,max}$ and $P_{T,min}$ are maximum- and minimum-rake average total pressures and $P_{T,av}$ is a face-average total pressure. All pressures are measured at station 2.

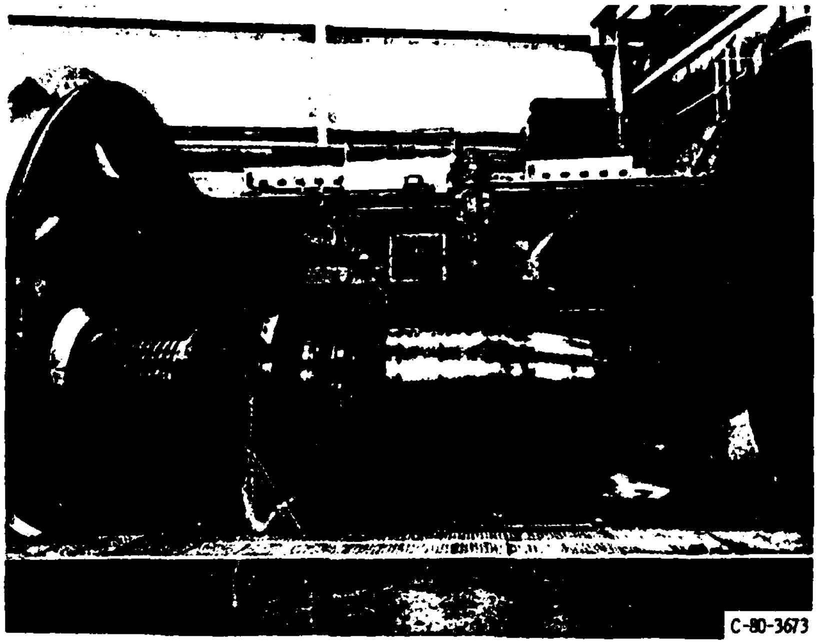

Figure 1. - TF-34 engine in altitude test chamber.

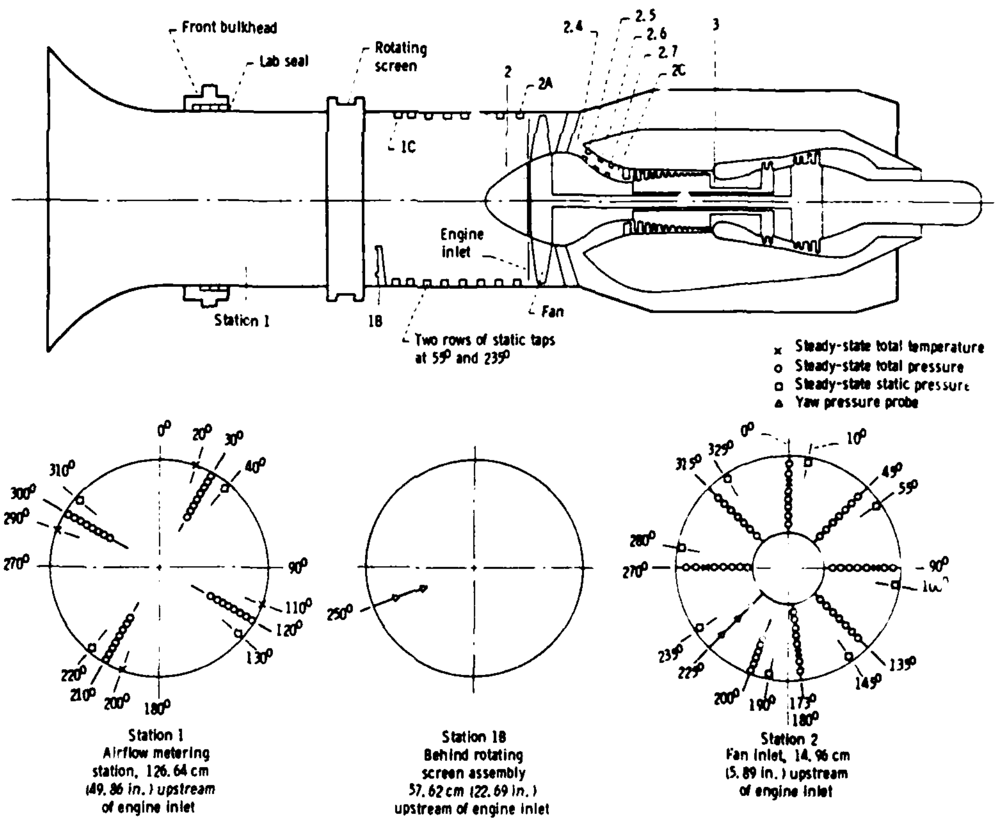

Figure 2. - Instrumentation layout for TF34 turbofan engine (stations viewed looking upstream).

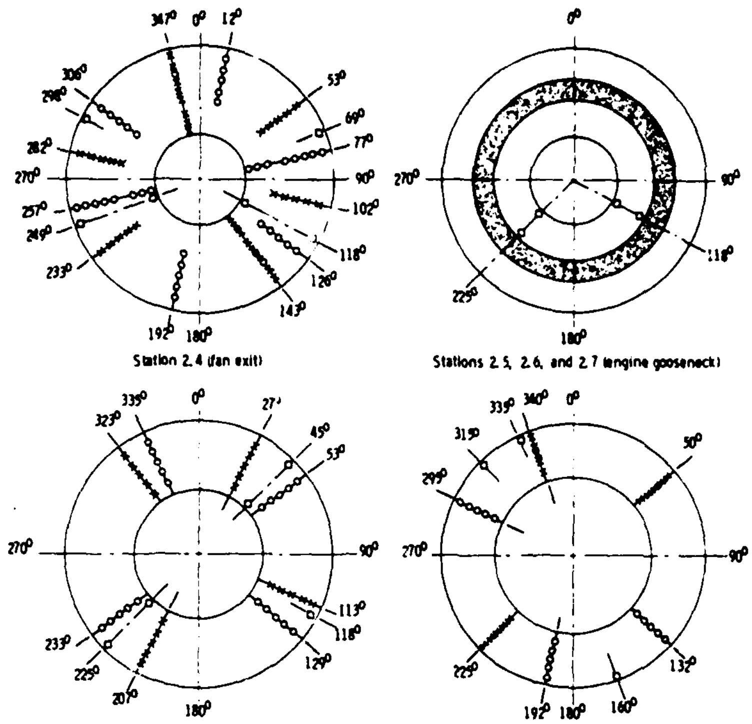

Figure 2. - Concluded.

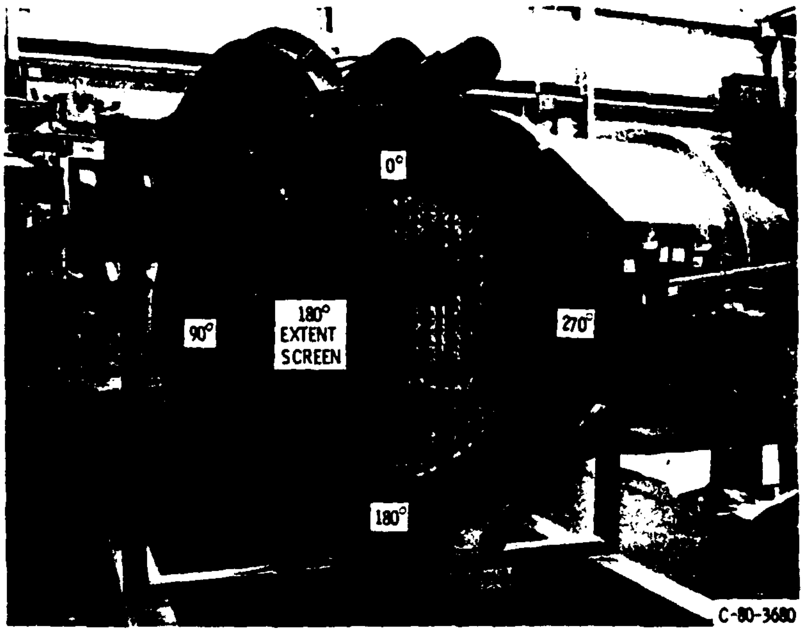

Figure 3. - Rotatable screen assembly, viewed in the direction of engine inlet.

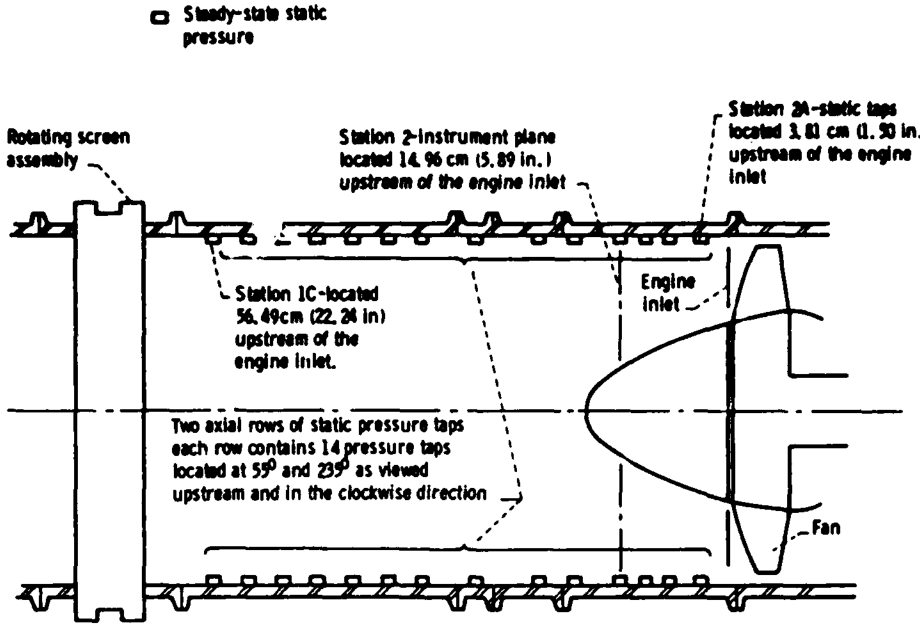

Figure 4. - Inlet ducting assembly.

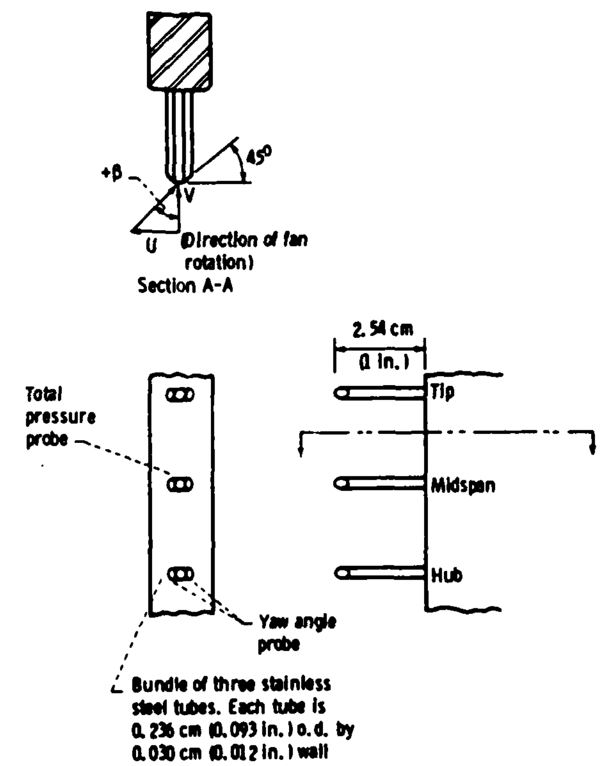

Figure 5. - Sketch of station 2 yaw-angle measurement rake.

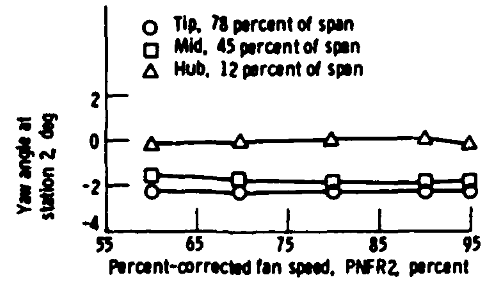

Figure 6. - Flow angle at station 2 (engine inlet) versus percent-corrected fan speed with no pressure distortion (clean inlet), 0.5 RNI.

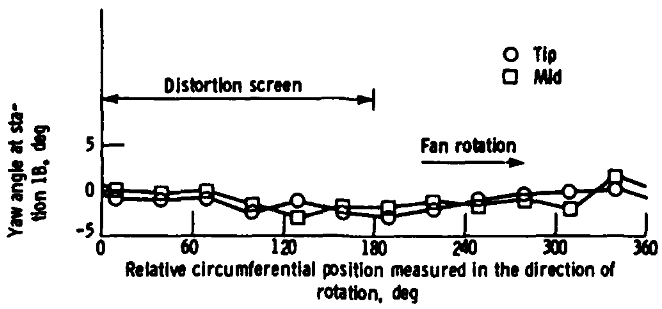

Figure 7. - Yaw-angle variation at station 1B (behind screen) for 180°, 49.4-percent blockage screen (9.8 percent total-pressure distortion). Corrected fan speed of 90 percent and 0.5 RNI.

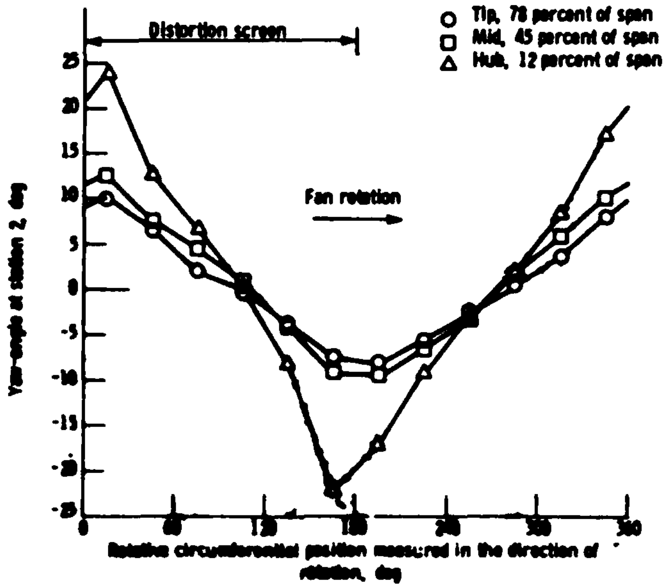

Figure 8. - Yaw-angle variation at station 2 for 180°, 49.4-percent blockage screen (9.8 percent total-pressure distortion). Corrected fan speed of 90 percent and 0.5 RNI.

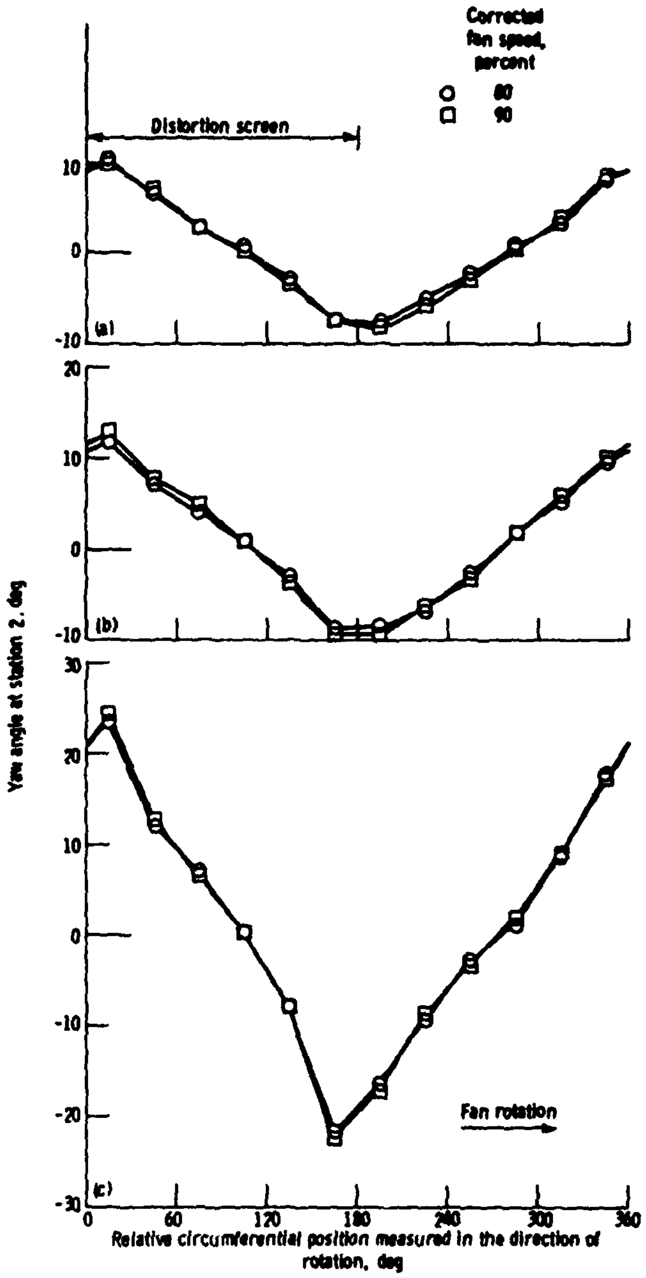

(a) Tip probe.

(b) Midspan probe.

(c) Hub probe.

Figure 9. - Effect of corrected fan speed in percent on yaw-angle variation at station 2 for 180°, 49.4-percent blockage (9.8 percent total-pressure distortion) with 0.5 RNI.

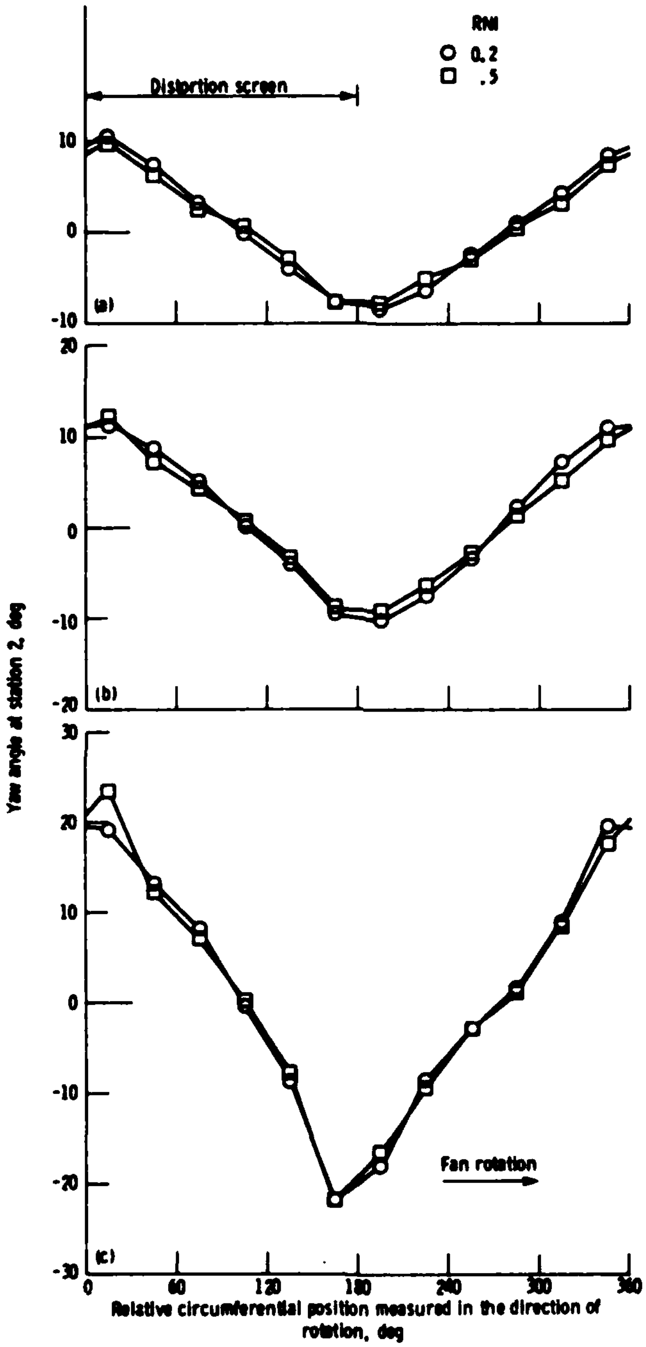

(a) Tip probe.

(b) Midspan probe.

(c) Hub probe.

Figure 10. - Effect of RNI on yaw-angle variation at station 2 for 180°, 49.4-percent blockage screen. Corrected fan speed is 80 percent.

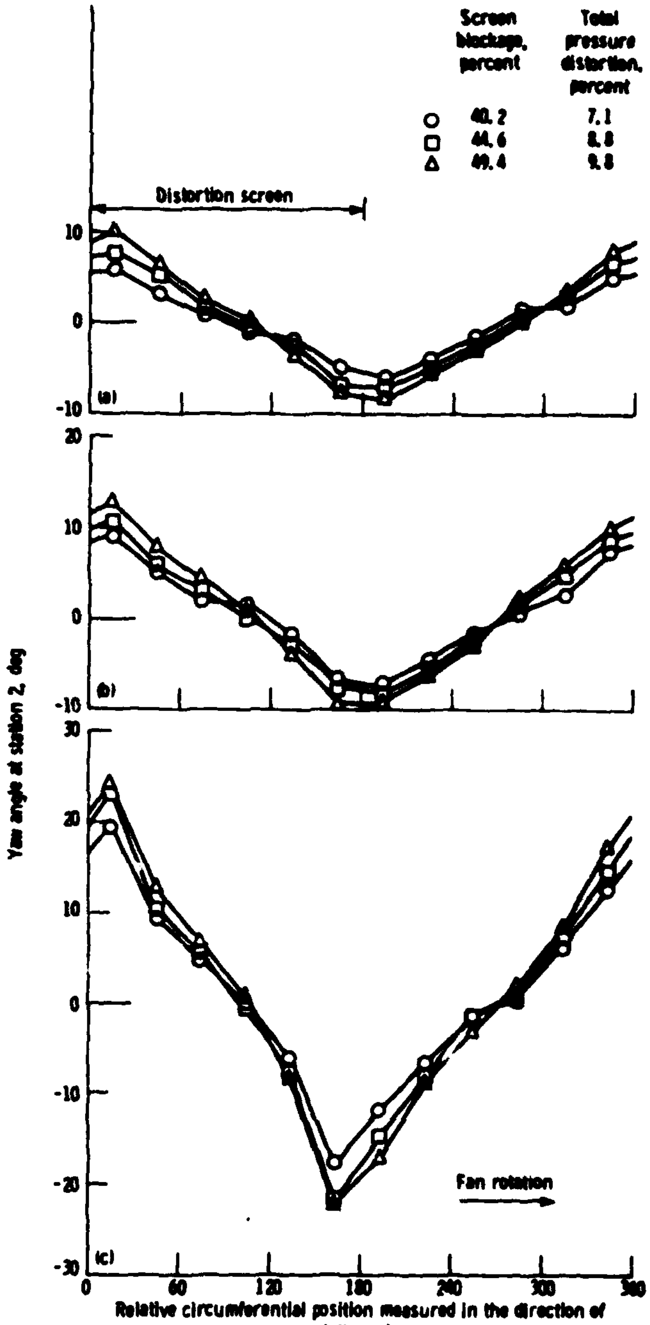

Relative circumferential position measured in the direction of rotation, deg

(a) Tip probe.

(b) Midspan probe.

(c) Hub probe.

Figure 11. - Comparison of three screen blockages of 180° on yaw-angle variation at station 2. Corrected fan speed of 90 percent and 0.5 RNI.

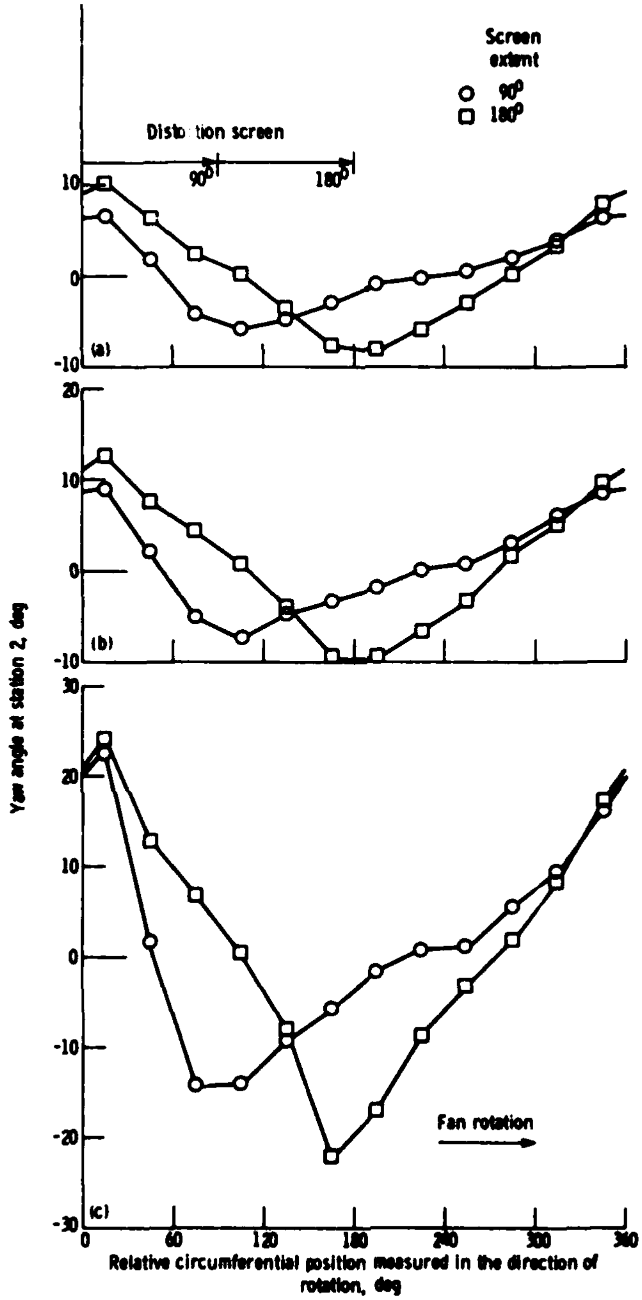

(a) Tip probe.

(b) Midspan probe.

(c) Hub probe.

Figure 12. - Effect of screen extent on yaw-angle variation at station 2 for a 49.4-percent blockage screen. Corrected fan speed of 90 percent and 0.5 RNI.

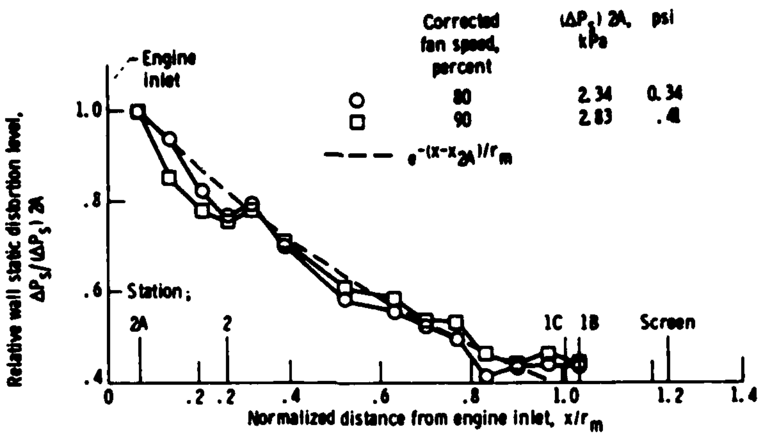

Figure 13. - Effect of percent-corrected fan speed on static pressure along inlet-duct wall for 180°, 49.4-percent blockage screen; 0.5 RNI.

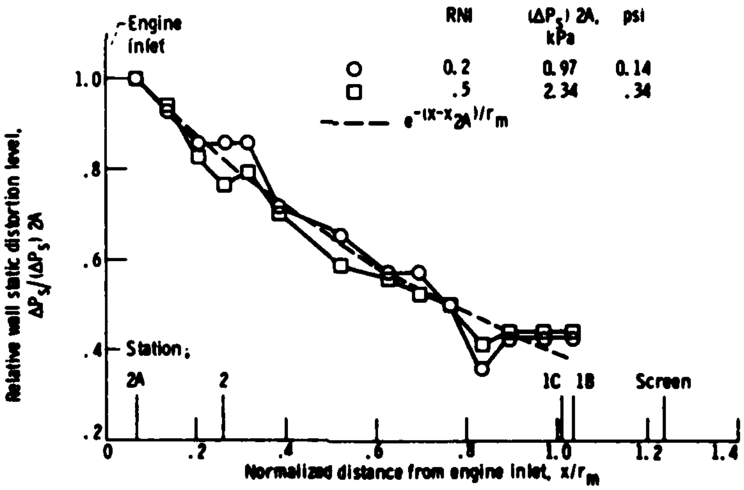

Figure 14. - Effect of RNI on static-pressure distortion along inlet-duct wall for 180°, 49.4-percent blockage screen; corrected fan speed, 80 percent.

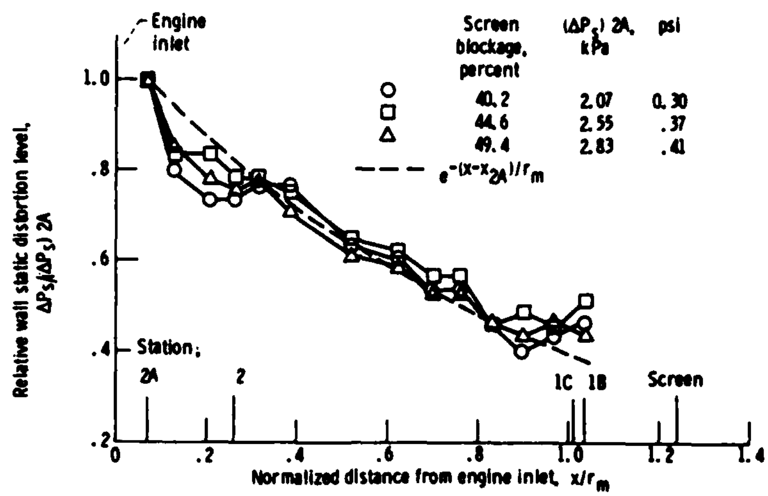

Figure 15. - Comparison of three screen blockages of 180° on static pressure distortion along inlet-duct wall. Corrected fan speed, 90 percent; 0.5 RNI.

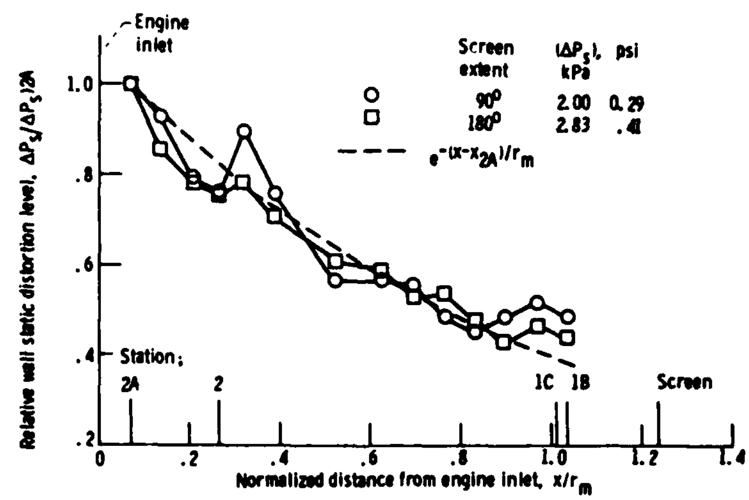

Figure 16. - Effect of screen extent on static-pressure distortion along inlet-duct wall. Corrected fan speed of 90 percent and 0.5 RNI.

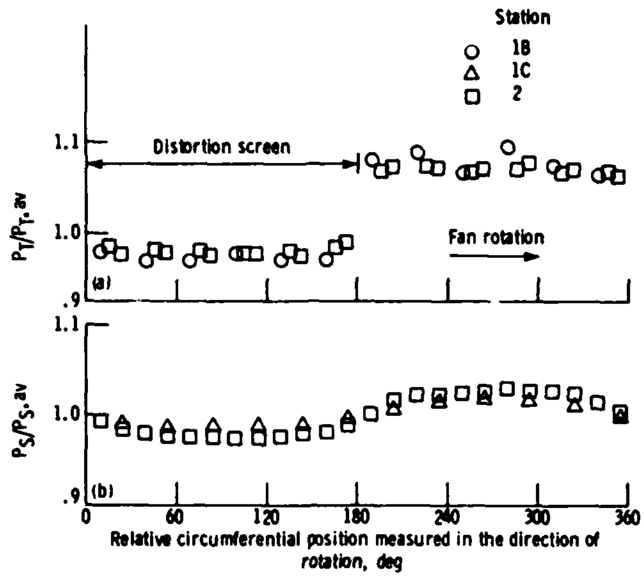

(a) Total pressure.

(b) Static pressure.

Figure 17. - Circumferential variation of total and static pressure with axial distance along inlet duct. Distortion screen is 180° and 49.4-percent blockage. Corrected fan speed, 90 percent; 0.5 RNI.

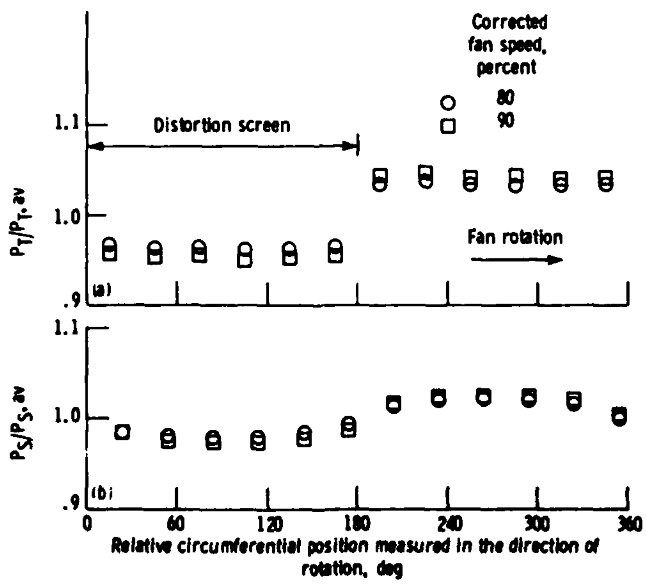

(a) Total pressure at station 2.

(b) Static pressure at station 2 (duct wall).

Figure 18. - Effect of corrected fan speed on circumferential total-and static-pressure variation for a 180°, 49.4-percent blockage screen.

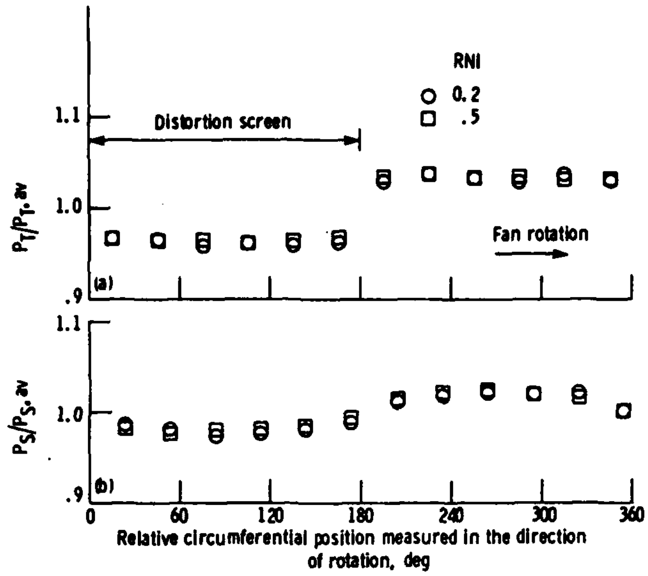

(a) Total pressure at station 2.

(b) Static pressure at station 2 (duct wall).

Figure 19. - Effect of RNI on circumferential total-and static-pressure variation for a 180°, 49.4-percent blockage screen. Corrected fan speed of 80 percent.

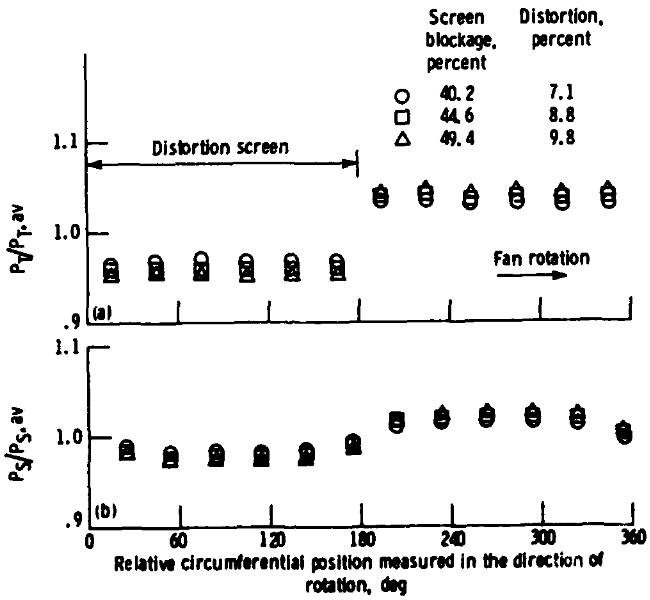

(a) Total pressure at station 2.

(b) Static pressure at station 2 (duct wall).

Figure 20. - Circumferential total-and static-pressure variation for a 180° screen of different blockages. Corrected fan speed of 90 percent and 0.5 RNI.

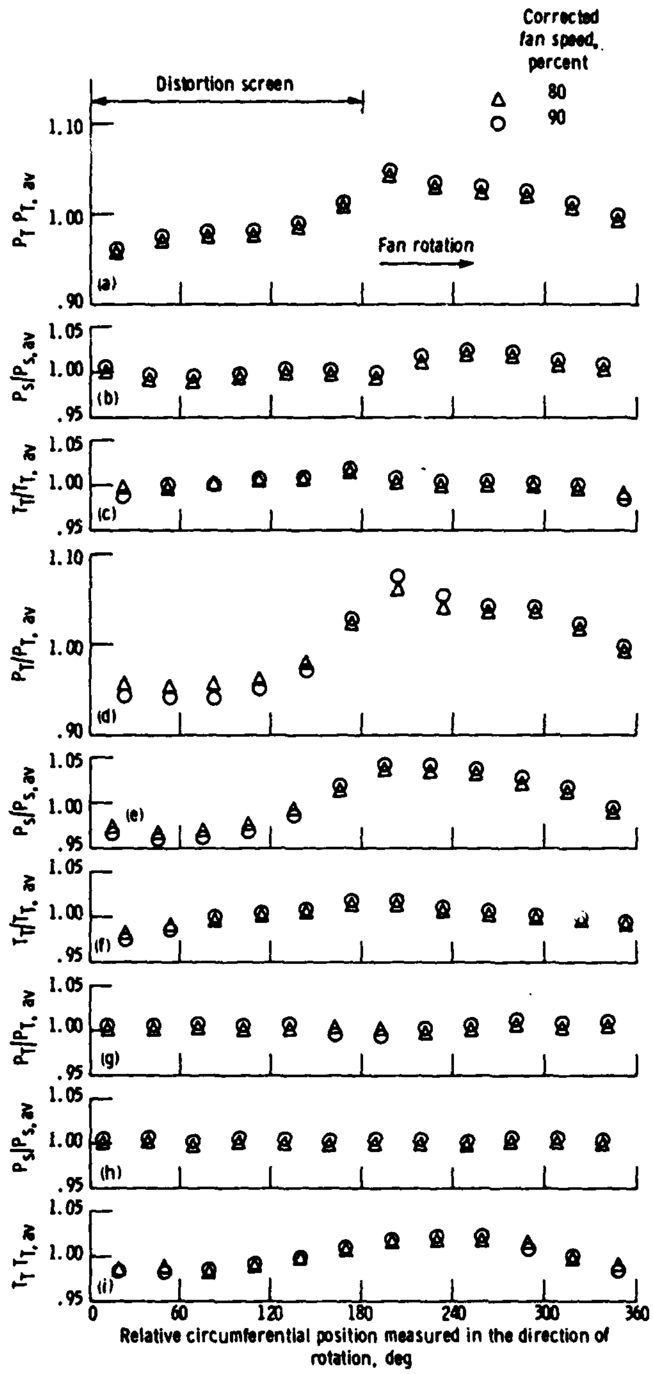

(a) Total pressure at station 2.4.

(b) Static pressure at station 2.4.

(c) Total temperature at station 2.4.

(d) Total pressure at station 2C.

(e) Static pressure at station 2C.

(f) Total temperature at station 2C.

(g) Total pressure at station 3.

(h) Static pressure at station 3.

(i) Total temperature at station 3.

Figure 21. - Effect of corrected fan speed on circumferential total- and static-pressure and total-temperature variation at stations 2.4, 2C, and 3. Distortion screen, 180°, 49.4-percent blockage; total-pressure distortion, 9.8 percent; 0.5 RNI.

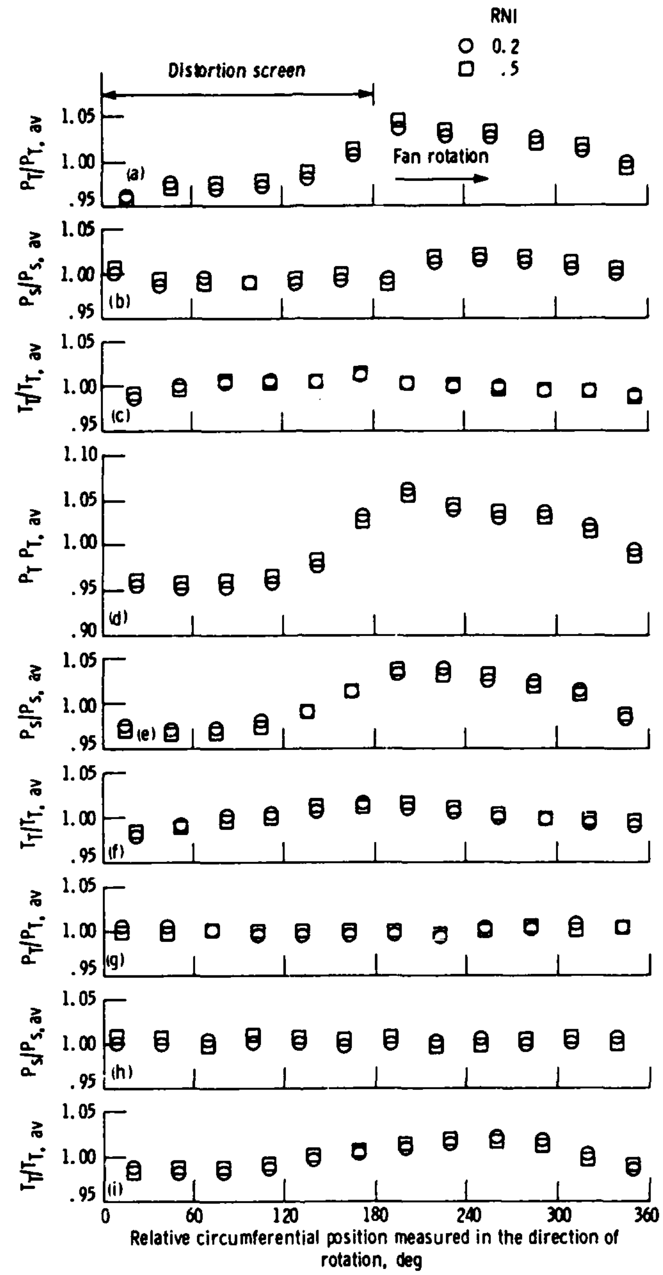

(a) Total pressure at station 2.4.

(b) Static pressure at station 2.4.

(c) Total temperature at station 2.4.

(d) Total pressure at station 2C.

(e) Static pressure at station 2C.

(f) Total temperature at station 2C.

(g) Total pressure at station 3.

(h) Static pressure at station 3.

(i) Total temperature at station 3.

Figure 22. - Effect of RNI on circumferential variation of total and static pressure and total temperature at stations 2.4, 2C, and 3. Distortion screen, 180°, 49.4 percent blockage; total-pressure distortion, 9.8 percent; corrected fan speed, 80 percent.

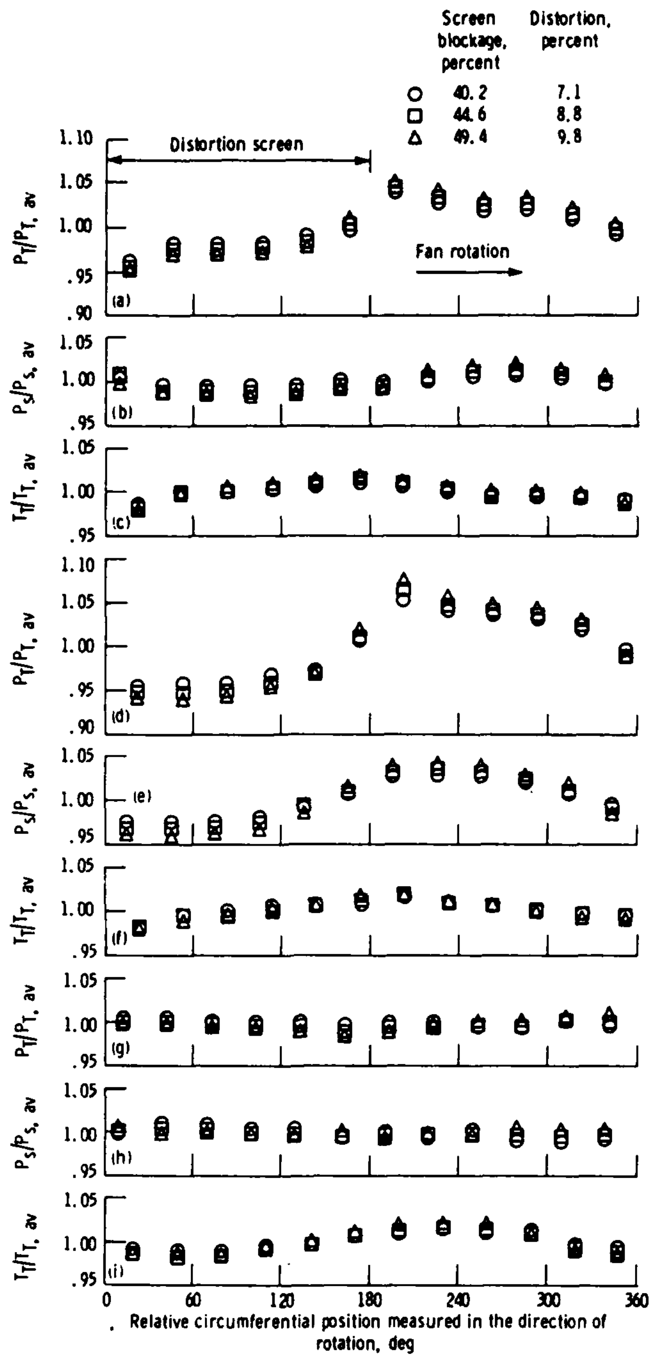

(a) Total pressure at station 2.4.

(b) Static pressure at station 2.4.

(c) Total temperature at station 2.4.

(d) Total pressure at station 2C.

(e) Static pressure at station 2C.

(f) Total temperature at station 2C.

(g) Total pressure at station 3.

(h) Static pressure at station 3.

(i) Total temperature at station 3.

Figure 23. - Circumferential variation of total and static pressure and total temperature at stations 2.4, 2C, and 3 for three screen blockages of 180°. Corrected fan speed of 90 percent and 0.5 RNI.

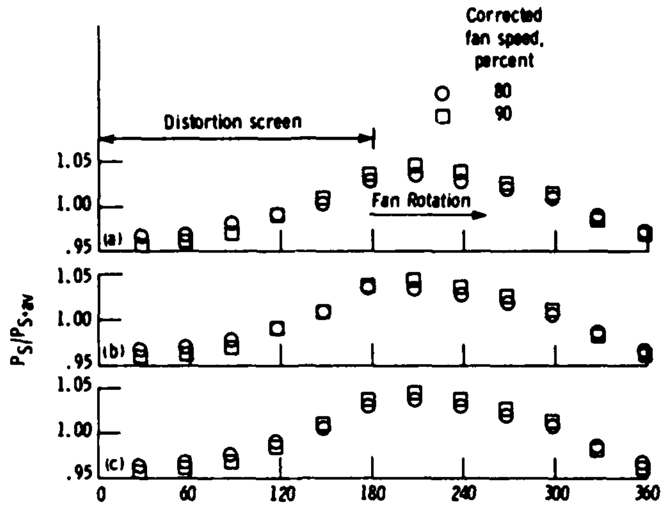

Relative circumferential position measured in the direction of rotation, deg

(a) Static pressure at station 2.5.

(b) Static pressure at station 2.6.

(c) Static pressure at station 2.7.

Figure 24. - Effect of percent-corrected fan speed on circumferential variation of static pressure at stations 2.5, 2.6, and 2.7 for 180°, 49.4-percent blockage screen; 0.5 RNI.

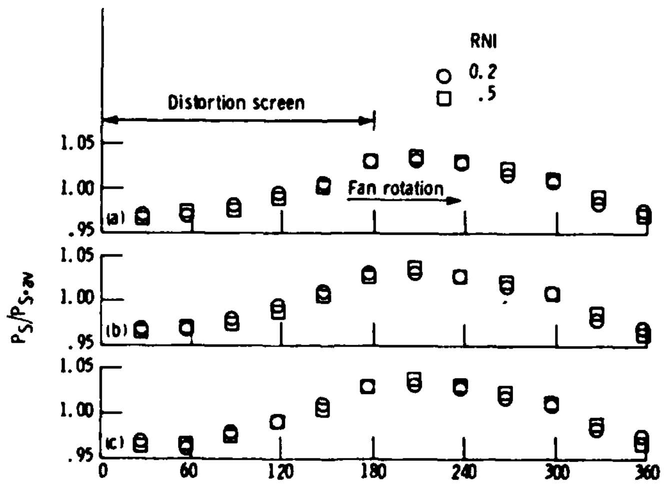

Relative circumferential position measured in the direction of rotation, deg

(a) Static pressure at station 2.5.

(b) Static pressure at station 2.6.

(c) Static pressure at station 2.7.

Figure 25. - Effect of RNI on circumferential variation of static-pressure at stations 2.5, 2.6, and 2.7 for 180°, 49.4 percent blockage screen; corrected fan speed, 90 percent.

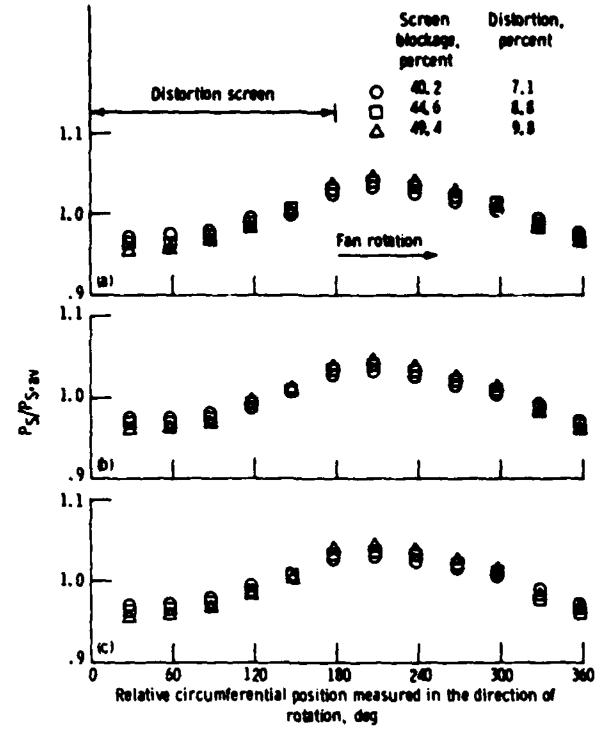

(a) Static pressure at station 2.5.

(b) Static pressure at station 2.6.

(c) Static pressure at station 2.7.

Figure 26. - *Circumferential variation of static pressure at stations 2.5, 2.6, and 2.7 for three screen blockages of 180° corrected fan speed, 90 percent; 0.5 RNI.*

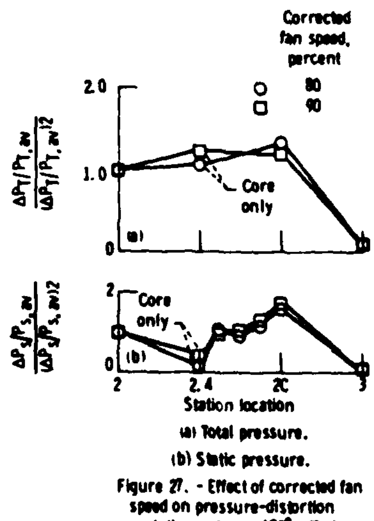

(a) Total pressure.

(b) Static pressure.

Figure 27. - Effect of corrected fan speed on pressure-distortion variation using a 180°, 49.4-percent blockage screen; 0.5 RNI.

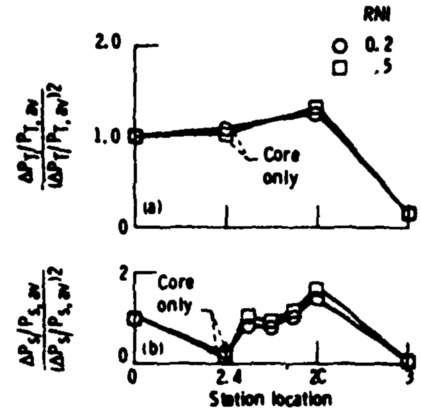

(a) Total pressure.

(b) Static pressure.

Figure 28. - Effect of RNI on pressure distortion variation for 180°, 49.4 percent blockage screen; corrected fan speed of 90 percent; 0.5 RNI.

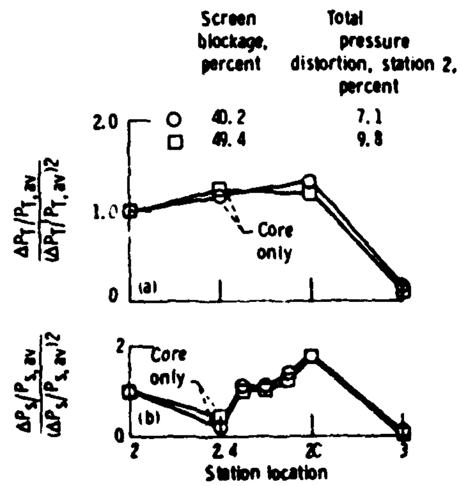

(a) Total pressure.

(b) Static pressure.

Figure 29. - Effect of screen blockage on pressure-distortion (at station 2) variation. Corrected fan speed, 90 percent; 0.5 RNI.

1. Report No. NASA TM-82964
AVRADCOM TR-81-C-27

2. Government Accession No.
A1-A123 807

3. Recipient's Catalog No.

4. Title and Subtitle
EFFECT OF STEADY-STATE PRESSURE DISTORTION ON INLET FLOW TO A HIGH-BYPASS-RATIO TURBOFAN ENGINE

5. Report Date

6. Performing Organization Code
505-32-6A

7. Author(s)
Ronald H. Soeder and George A. Bobula

8. Performing Organization Report No.
E-1383

9. Performing Organization Name and Address
NASA Lewis Research Center and
AVRADCOM Research and Technology Laboratories
Cleveland, Ohio 44135

10. Work Unit No.

11. Contract or Grant No.

12. Sponsoring Agency Name and Address
National Aeronautics and Space Administration
Washington, D.C. 20546 and U.S. Army Aviation Research and Development Command, St. Louis, Mo. 63166

13. Type of Report and Period Covered
Technical Memorandum

14. Sponsoring Agency Code

15. Supplementary Notes
Ronald H. Soeder, NASA Lewis Research Center; George A. Bobula, Propulsion Laboratory, AVRADCOM Research and Technology Laboratories, Lewis Research Center, Cleveland, Ohio 44135.

16. Abstract

Static-pressure and total-pressure distributions were measured in the inlet duct upstream of the engine inlet and within the fan and compressor of a YTF34 turbofan engine. In addition, the free-stream flow angle was measured between the distortion generator and the engine inlet. Distortions were generated using three screen configurations with extents of 90° or 180°. The screens were mounted on a rotatable screen assembly. Reynolds number index upstream of the distortion device was maintained at 0.5 or 0.2, and engine fan speed corrected to station 2 temperature was maintained at 80 or 90 percent of rated condition (7005 rpm). Flow angle was nearly constant near the distortion device and increased as flow approached the engine inlet. The largest flow angle occurred in the hub region of the engine inlet. Static-pressure distortion along the inlet duct increased exponentially as the flow approached the engine. Both static-pressure and total-pressure distortions were attenuated between engine inlet and compressor exit.

17. Key Words (Suggested by Author(s))
High-bypass-ratio turbofan engine
Inlet flow angle
Inlet and internal static-pressure distortion
Inlet and internal total-pressure distortion

18. Distribution Statement
Unclassified - unlimited
STAR Category 07

19. Security Classif. (of this report)	20. Security Classif. (of this page)	21. No. of Pages	22. Price*
Unclassified	Unclassified		

* For sale by the National Technical Information Service, Springfield, Virginia 22161